

## Article

# Influence of Cr, Mn, Co and Ni Addition on Crystallization Behavior of Al<sub>13</sub>Fe<sub>4</sub> Phase in Al-5Fe Alloys Based on ThermoDynamic Calculations

Na Pang \*, Zhiming Shi \*, Cunquan Wang, Ninyu Li and Yaming Lin

School of Materials Science and Engineering, Inner Mongolia University of Technology, Hohhot 010051, China; wccq94810@163.com (C.W.); liningyu518@163.com (N.L.); liny00@163.com (Y.L.)

\* Correspondence: pangna@imut.edu.cn (N.P.); shizm@imut.edu.cn (Z.S.); Tel.: +86-471-657-5752 (N.P.); +86-471-657-5752 (Z.S.)

**Abstract:** Alloying is an effective method to refine coarse grains of an Al<sub>13</sub>Fe<sub>4</sub> phase and strengthen Al-Fe alloys. However, the grain refinement mechanism remains unclear in terms of the thermodynamics. Herein, the influence of *M*-element, i.e., Cr, Mn, Co and Ni, addition on the activity of Al and Fe atoms, Gibbs free energy of the Al<sub>13</sub>Fe<sub>4</sub> nucleus in Al-Fe melt and the formation enthalpy of an Al<sub>13</sub>Fe<sub>4</sub> phase in Al-Fe alloys is systematically investigated using the extended Miedema model, Wilson equation, and first-principle calculations, respectively. The results reveal that the addition of different *M* elements increases the activity of Fe atoms and reduces the Gibbs free energy of the Al<sub>13</sub>Fe<sub>4</sub> nucleus in Al-Fe melt, where the incorporation of Ni renders the most obvious effect, followed by Mn, Co, and Cr. Additionally, the formation enthalpy decreases in the following order: Al<sub>78</sub>(Fe<sub>23</sub>Cr) > Al<sub>78</sub>(Fe<sub>23</sub>Mn) > Al<sub>13</sub>Fe<sub>4</sub> > Al<sub>78</sub>(Fe<sub>23</sub>Ni) > Al<sub>78</sub>(Fe<sub>23</sub>Co), where the formation enthalpy of Al<sub>78</sub>(Fe<sub>23</sub>Ni) is close to Al<sub>78</sub>(Fe<sub>23</sub>Co). Moreover, the presence of Ni promotes the nucleation of the Al<sub>13</sub>Fe<sub>4</sub> phase in Al-Fe alloys, which reveals the mechanism of grain refinement from a thermodynamics viewpoint.

**Keywords:** Al<sub>13</sub>Fe<sub>4</sub> phase; 3d transition elements; Gibbs free energy; formation enthalpy; crystallization behavior



**Citation:** Pang, N.; Shi, Z.; Wang, C.; Li, N.; Lin, Y. Influence of Cr, Mn, Co and Ni Addition on Crystallization Behavior of Al<sub>13</sub>Fe<sub>4</sub> Phase in Al-5Fe Alloys Based on ThermoDynamic Calculations. *Materials* **2021**, *14*, 768. <https://doi.org/10.3390/ma14040768>

Academic Editor: Werner Skrotzki

Received: 9 January 2021

Accepted: 3 February 2021

Published: 6 February 2021

**Publisher's Note:** MDPI stays neutral with regard to jurisdictional claims in published maps and institutional affiliations.



**Copyright:** © 2021 by the authors. Licensee MDPI, Basel, Switzerland. This article is an open access article distributed under the terms and conditions of the Creative Commons Attribution (CC BY) license (<https://creativecommons.org/licenses/by/4.0/>).

## 1. Introduction

Al-Fe alloys are promising candidates for high-temperature applications due to the presence of a thermodynamically stable Al<sub>13</sub>Fe<sub>4</sub> phase in the aluminum (Al) matrix [1,2]. However, the mechanical properties of Al-Fe alloys are compromised due to the coarse flake-like, needles and laths of the Al<sub>13</sub>Fe<sub>4</sub> phase [3–5]. To date, different approaches have been adopted to enhance the mechanical properties of Al-Fe alloys by reducing the grain size and improving the morphology and distribution of the Al<sub>13</sub>Fe<sub>4</sub> phases.

Transition metals are widely used as dopants due to their low solid solubility and diffusion rate in Al-based alloys [6], forming coarsening-resistant intermetallics, such as ternary Al-Fe-X alloys (X = Zr, Mo, Si, Ni and Cr). These ternary Al-Fe-X alloys render high strength at temperatures up to 400 °C [7,8]. For instance, the addition of Ni refines the Al<sub>13</sub>Fe<sub>4</sub> phase and promotes the formation of orthorhombic Al<sub>3</sub>Ni and monoclinic Al<sub>9</sub>FeNi phases [8–10], improving the high-temperature mechanical properties and decreasing the thermal expansion coefficient (TEC) of the Al-Fe alloys [11,12]. Additionally, instead of forming an AlCr binary compound, Cr prefers to dissolve in the Al<sub>13</sub>Fe<sub>4</sub> phase and improve the morphology, whereas the presence of Mn stabilizes the metastable Al<sub>6</sub>Fe phase and forms an Al<sub>6</sub>(Fe,Mn) solid-solution. With the increase in Cr content, the morphology of the Al<sub>13</sub>Fe<sub>4</sub> phase changes from a needle-like structure to poly-angled and sheet-like structures in Al-5Fe alloys [13]. Furthermore, the addition of Mn increases the yield strength and ultimate tensile strength of Al-Fe alloys, however, the elongation is compromised due to

the formation of a large volume fraction of Fe- and Mn-bearing intermetallics, in addition to crack propagation [14]. It has been reported that the addition of 0.2 wt% Co completely dissolved in the  $\text{Al}_{13}\text{Fe}_4$  phase and significantly improved the morphology of the  $\text{Al}_{13}\text{Fe}_4$  phase in Al-5Fe alloys [15].

These experimental studies demonstrate the prominent influence of alloying on the grain refinement of an  $\text{Al}_{13}\text{Fe}_4$  phase and the mechanical properties of Al-Fe alloys. One should note that the reinforcement effect of the  $\text{Al}_{13}\text{Fe}_4$  phase in Al-Fe alloys depends on nucleation and coarsening, which are influenced by the changes in the formation enthalpy and Gibbs free energy. The alloying elements influence the Gibbs free energy by altering the component activity in the Al-Fe melt and affect the formation enthalpy by forming a solid-solution. The decrease in Gibbs free energy and formation enthalpy facilitates phase transformation, sub-cooling degree and nucleation rate, promoting the reinforcement of the  $\text{Al}_{13}\text{Fe}_4$  phase. However, the component activity, Gibbs free energy and formation enthalpy of multicomponent melts are rarely reported due to the complex and extended lab-scale experiments involved.

Therefore, it is of utmost significance to develop a theoretical approach to screen alloying elements for the refinement of the  $\text{Al}_{13}\text{Fe}_4$  phase. Herein, theoretical calculations are used to investigate the influence of M addition, where M refers to Cr, Mn, Co, or Ni, on the Gibbs free energy and formation enthalpy of the  $\text{Al}_{13}\text{Fe}_4$  phase. First, the effect of M incorporation on the activity of Al and Fe atoms and the Gibbs free energy of the  $\text{Al}_{13}\text{Fe}_4$  phase in an Al-Fe melt is estimated by using the extended Miedema model and Wilson equation, respectively. Second, the influence of M addition on the formation enthalpy of the  $\text{Al}_{13}\text{Fe}_4$  phase is assessed using the first-principle calculations. Third, the microstructural evolution of Al-Fe alloys with the addition of Ni and Cr is investigated based on theoretical predictions. The current study aimed to reveal the mechanism of grain refinement of the  $\text{Al}_{13}\text{Fe}_4$  phase due to the addition of 3D transition elements from a thermodynamics viewpoint.

## 2. Calculations and Experimental Procedures

### 2.1. Change in Gibbs Free Energy of Al-Fe Melt

A hypereutectic Al-5wt%Fe (Al-2.47at%Fe) alloy and corresponding melt (at 850 °C) were selected as objects for thermodynamics calculations, where the melt temperature was slightly greater than the crystallization temperature. The formation of a coarse  $\text{Al}_{13}\text{Fe}_4$  phase can be given as:



The change in Gibbs free energy during the formation of primary  $\text{Al}_{13}\text{Fe}_4$  phase can be expressed as:

$$\Delta G_{\text{Al}_{13}\text{Fe}_4}^1 = \Delta G_{\text{Al}_{13}\text{Fe}_4}^0 - 13RT \ln a_{\text{Al}} - 4RT \ln a_{\text{Fe}}, \quad (2)$$

where  $\Delta G_{\text{Al}_{13}\text{Fe}_4}^0$  refers to the standard Gibbs energy of formation,  $a_i$  represents the component activity,  $R$  corresponds to a gas constant and  $T$  denotes the absolute temperature of the Al-Fe melt. The activity of the  $\text{Al}_{13}\text{Fe}_4$  solid in the melt can be considered as 1.

The incorporation of the M element forms a ternary Al-Fe-M system, where the activity of both Al and Fe atoms is also altered. Therefore, Equation (2) can be rearranged as:

$$\begin{aligned} \Delta G_{\text{Al}_{13}\text{Fe}_4}^2 &= \Delta G_{\text{Al}_{13}\text{Fe}_4}^0 - 13RT \ln(a_{\text{Al}} + \Delta a_{\text{Al}}) - 4RT \ln(a_{\text{Fe}} + \Delta a_{\text{Fe}}) \\ &= \Delta G_{\text{Al}_{13}\text{Fe}_4}^0 - 13RT \ln(x_{\text{Al}} + \Delta x_{\text{Al}})(r_{\text{Al}} + \Delta r_{\text{Al}}) - 4RT \ln(x_{\text{Fe}} + \Delta x_{\text{Fe}})(r_{\text{Fe}} + \Delta r_{\text{Fe}}), \\ &= \Delta G_{\text{Al}_{13}\text{Fe}_4}^0 - 13RT \ln(1 + P_{\text{Al}})(1 + Q_{\text{Al}}) - 4RT \ln(1 + P_{\text{Fe}})(1 + Q_{\text{Fe}}) \end{aligned} \quad (3)$$

where  $a_i = x_i \cdot r_i$ ,  $x_i$  represents the atomic fraction of component  $i$  in the melt and  $\gamma_i$  refers to the activity coefficient.  $\Delta x_i$  and  $\Delta r_i$  represent the change in component concentration and activity coefficient, respectively. Additionally,  $P_i$  and  $Q_i$  can be given as:

$$P_i = \frac{\Delta x_i}{x_i}, Q_i = \frac{\Delta r_i}{r_i}, \quad (4)$$

Then, using the prediction model, the activity coefficient in a multicomponent system can be theoretically calculated. Combining Equations (2) and (3), the Gibbs free energy change,  $\Delta G$ , can be calculated with alloying elements additions. Therefore, the influence of alloying element additions on the chemical reaction can be determined.

The aforementioned theoretical models for calculating chemical activity are usually suitable for binary alloys. Fan et al. [16–18] utilized Wilson's equation [19] to propose a novel method for calculating the activity of components in a multicomponent melt. According to the extended Miedema model [20] and Wilson equation [19], which only relies on the physical parameters of alloying elements, the reliability of this method was well verified in Al-Mg-X (X=Si, Mn, Cu, Zn), Al-Ti-B, Al-Ti-B-X (X=Mg, Si, Cu, Zr, V, Fe, Ni, La) systems [16,17,21].

According to the thermodynamic model, introduced by Fan et al., the activity coefficient ( $\gamma_i$ ) in  $i$ ,  $j$ , and  $k$  ternary systems can be given as:

$$\ln \gamma_i = 1 - \ln(1 - x_j A_{j/i} - x_k A_{k/i}) - \frac{x_i}{1 - x_j A_{j/i} - x_k A_{k/i}} - \frac{x_j(1 - A_{i/j})}{1 - x_i A_{i/j} - x_k A_{k/j}} - \frac{x_k(1 - A_{i/k})}{1 - x_i A_{i/k} - x_j A_{j/k}}, \quad (5)$$

where  $A_{ij}$  and  $A_{ji}$  are adjustable parameters. The pair of parameters, i.e.,  $A_{ij}$  and  $A_{ji}$ , can be calculated by  $\ln \gamma_i^{x_i \rightarrow 0}$  and  $\ln \gamma_j^{x_j \rightarrow 0}$ ; which are based on the binary infinitely dilute activity coefficients, as given below:

$$\ln \gamma_i^{x_i \rightarrow 0} = -\ln(1 - A_{j/i}) + A_{i/j}, \quad (6)$$

$$\ln \gamma_j^{x_j \rightarrow 0} = -\ln(1 - A_{i/j}) + A_{j/i}, \quad (7)$$

According to the Miedema model and thermodynamics model, the activity coefficient of component  $i$  in an infinite solution  $j$  can be given as:

$$\ln \gamma_i^{x_i \rightarrow 0} = \frac{\alpha_{ij} f_{ij} [1 + u_i(\varphi_i - \varphi_j)]}{RTV_j^{\frac{2}{3}}}, \quad (8)$$

Here,  $\alpha_{ij}$  and  $f_{ij}$  are defined as:

$$\alpha_{ij} = 1 - 0.1T \left( \frac{1}{T_{m_i}} + \frac{1}{T_{m_j}} \right) \quad (9)$$

$$f_{ij} = \frac{2pV_i^{\frac{2}{3}}V_j^{\frac{2}{3}} \left\{ q/p \left[ \left( n_{ws}^{\frac{1}{3}} \right)_i - \left( n_{ws}^{\frac{1}{3}} \right)_j \right]^2 - (\varphi_i - \varphi_j)^2 - b(r/p) \right\}}{\left( n_{ws}^{\frac{1}{3}} \right)_i^{-1} + \left( n_{ws}^{\frac{1}{3}} \right)_j^{-1}} \quad (10)$$

The advantage of this method is that, independent of the experimental data, it is applicable to multiple liquid alloys and capable of predicting thermodynamic data according to the physical parameters of these elements. In Equations (8)–(10),  $T_{m_i}$  and  $T_{m_j}$  represent the melting temperature of component  $i$  and  $j$ , respectively;  $\varphi$  refers to electronegativity in volts;  $n_{ws}$  denotes the electron density at the boundary of the Wigner–Seitz cell in density units (d.u.,

about  $6 \times 10^{22}$  electrons/cm<sup>3</sup>);  $V$  refers to the molar volume in cm<sup>3</sup>/mol, and  $u$  is a constant. For all alloys,  $q/p$  is equal to  $9.4 \text{ V}^2/(\text{d.u.})^{2/3}$ . The values of  $p$  for alloys of two transition metals, two non-transition metals, and a transition metal with a non-transition metal are 14.2, 10.7 and 12.35, respectively. The term  $b$  for the solid, liquid alloy with a transition metal and a non-transition metal, and other alloys is equal to 1.0, 0.73 and 0, respectively.

## 2.2. Formation Enthalpy of Al<sub>13</sub>Fe<sub>4</sub> Phase Based on First-Principle Calculations

### 2.2.1. Crystal Structure of Al<sub>13</sub>Fe<sub>4</sub>

The preliminary X-ray diffraction results suggest that the Al<sub>13</sub>Fe<sub>4</sub> compound possesses a monoclinic structure with a complex bottom center [22–24], which belongs to the space group C2/m. The unit cell of Al<sub>13</sub>Fe<sub>4</sub> is composed of twenty crystallographically different atomic species shown in Table 1, containing 15 different Al atoms and 5 different Fe atoms ( $a = 15.489 \text{ \AA}$ ,  $b = 8.0831 \text{ \AA}$ ,  $c = 12.476 \text{ \AA}$ ,  $\beta = 107.72^\circ$ ). In total, 102 atoms (78 Al and 24 Fe) are shown in Figure 1. The coordination number of Fe-1, Fe-2 and Fe-5 is 11, 10 and 9, respectively, whereas the coordination number of Fe-3 and Fe-4 is 10 with Al and 1 with Fe [22].

**Table 1.** Atomic parameters in Al<sub>13</sub>Fe<sub>4</sub> [22].

Atom	x/a	y/b	z/c	No. in Cell	Atom	x/a	y/b	z/c	No. in Cell
Al1	0	0.5	0.5	2	Al11	0.1883	0.2164	0.1111	8
Al2	0	0.2441	0	4	Al12	0.3734	0.2110	0.1071	8
Al3	0.3223	0	0.2778	4	Al13	0.1765	0.2168	0.3343	8
Al4	0.2352	0	0.5392	4	Al14	0.4959	0.2832	0.3296	8
Al5	0.0812	0	0.5824	4	Al15	0.3664	0.2238	0.4799	8
Al6	0.2317	0	0.9729	4	Fe1	0.0865	0	0.3831	4
Al7	0.4803	0	0.8277	4	Fe2	0.4018	0	0.6243	4
Al8	0.3100	0	0.7695	4	Fe3	0.0907	0	0.9890	4
Al9	0.0869	0	0.7812	4	Fe4	0.4001	0	0.9857	4
Al10	0.0645	0	0.1730	4	Fe5	0.3188	0.2850	0.2770	8

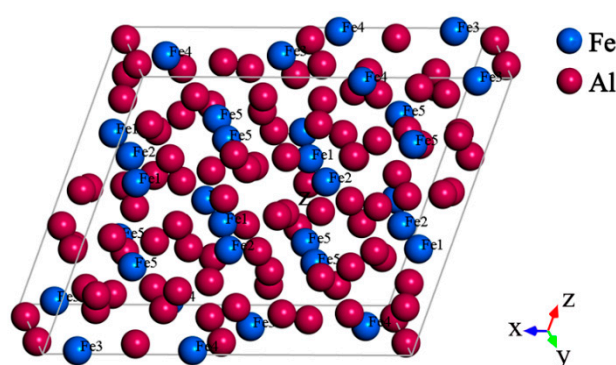


**Figure 1.** The unit cell of the Al<sub>13</sub>Fe<sub>4</sub> compound.

### 2.2.2. Computational Details

The calculations were performed via the Materials Studio program using the Cambridge sequential total energy package (CASTEP) based on the density-functional theory (DFT) [25], where a combination of generalized gradient approximation (GGA) and Perdew–Burke–Ernzerhof (PBE) was employed to the electronic exchange–correlation energy [26], and the ultra-soft pseudopotential was employed to describe ionic interactions [27].

Based on the convergence test, the  $k$ -point of Al<sub>13</sub>Fe<sub>4</sub> and Al<sub>78</sub>(Fe<sub>23</sub>M) compound was set as  $2 \times 3 \times 2$ , which was generated by the Monkhorst–Pack scheme [28]. The substituted compounds are represented by the actual number of atoms in a cell. The cut-off energy was set at 400 eV. The self-consistent field (SCF) method was employed to calculate the total energy based on the Pulay density mixing method. The geometric optimization was

performed using the Broyden–Fletcher–Goldfarb–Shanno (BFGS) method to obtain the most stable structure [29]. Herein, the total energy of  $10^{-5}$  eV/atom and the maximum force tolerance of  $0.03$  eV/Å were set for optimization.

Moreover, the formation enthalpy of  $\text{Al}_{78}(\text{Fe}_{23}\text{M})$  under different spin directions and spin states was calculated. The results revealed that the consideration of magnetism rendered a negligible influence and the effect of four elements on the  $\text{Al}_{78}(\text{Fe}_{23}\text{M})$  phase remained unchanged. Therefore, the spin polarization was not considered because it is unnecessary for such Al-rich complex intermetallic compounds [30]. Hence, the magnetism was not considered in subsequent calculations to optimize the utilization of available computing resources.

The formation enthalpy ( $\Delta H$ ) of  $\text{Al}_{78}(\text{Fe}_{23}\text{M})$  ( $M = \text{Cr}, \text{Mn}, \text{Co}$  or  $\text{Ni}$ ) alloys at 0 K can be defined as:

$$\Delta H = \frac{1}{102} (E_{tot}^{\text{Al}_{78}(\text{Fe}_{23}\text{M})} - 78E_{solid}^{\text{Al}} - 23E_{solid}^{\text{Fe}} - E_{solid}^{\text{M}}), \quad (11)$$

where  $E_{tot}^{\text{Al}_{78}(\text{Fe}_{23}\text{M})}$ ,  $E_{solid}^{\text{Al}}$ ,  $E_{solid}^{\text{Fe}}$  and  $E_{solid}^{\text{M}}$  represent the total energy of the  $\text{Al}_{78}(\text{Fe}_{23}\text{M})$ , Al, Fe and M ( $M = \text{Cr}, \text{Mn}, \text{Co}, \text{Ni}$ ), respectively.

### 2.3. Experimental Details

To confirm the effectiveness of M addition on grain refinement of the  $\text{Al}_{13}\text{Fe}_4$  phase, an Al-5wt%Fe alloy was prepared by melting pure aluminum (99.7 wt. %) and master alloys of Al-20wt%Fe, Al-10wt%Ni and Al-5wt%Cr to prepare Al-5wt%Fe-1wt%M ( $M = \text{Ni}$  and  $\text{Cr}$ ), respectively. For each composition, the aluminum ingot was melted in an electrical resistance furnace and the Al-20wt%Fe ingot was added to form the Al-5wt%Fe melt, at  $880$  °C for 40 min. Then, different amounts of Al-10wt%Ni and Al-5wt%Cr master alloys were added into the molten alloy and the melts were stirred for 15 min using a graphite stirrer. The nitrogen was utilized to eliminate gases and avoid oxidation of the alloy melt. When the temperature decreased to  $850$  °C, the melts were poured into bars ( $\Phi 35 \times 25$  mm) for microstructural observations.

The as-cast ingots were cooled down to room temperature in the mold and sectioned at the tip in the thermocouple sheath. The metallographic samples were rubbed with sandpaper and then polished with a polishing machine. Five micrograph views were chosen for length measurement of  $\text{Al}_{13}\text{Fe}_4$ . Each view obtained around 50 data points for average calculation. For each component, three samples were prepared and microstructural observations were carried out from the same position at the thermocouple tip. A scanning electron microscope (SEM, S3400-N, Hitachi, Tokyo, Japan) at an accelerating voltage of 20 kV under high vacuum, equipped with a 7021-H/Horiba energy dispersive spectrometer (EDS, Kyodo, Japan), was adopted to observe the morphology and analyze the elemental distribution. A D/MAX-2500/PC/PIGAKV X-ray diffractometer (XRD, Rigaku corporation, Tokyo, Japan), equipped with a Cu  $\alpha$  target, was employed to analyze the phase composition. XRD patterns were recorded in the  $2\theta$  range of  $20^\circ$  to  $70^\circ$  at the scan speed of  $3^\circ/\text{min}$ .

## 3. Results and Discussion

### 3.1. Gibbs Free Energy of $\text{Al}_{13}\text{Fe}_4$ Nucleus in Al-Fe Melt

The component activity is an important factor in determining thermodynamic stability of the reaction between the  $\text{Al}_{13}\text{Fe}_4$  phase and the Al matrix in liquid alloys. Thus, it is vital to understand this mechanism theoretically and thereby control it favorably, especially in a multiple-component system. When the Al-Fe melt includes alloying components, based on Equation (5), the investigation on the influence of alloying element additions on the chemical stability of Equation (1) can be divided into two aspects: (i) the variation  $P_i$  of component concentration in the composite melt, and (ii) the impact factor  $Q_i$  on activity coefficients of Al and Fe. Al-Fe-M alloy composites, such as alloy melt, at high temperatures can be described as an Al-Fe-M ternary liquid alloy system when the chemical reaction in

Equation (1) takes place. The values of the parameters required are presented in Table 2 [31], and according to Equations (6)–(9), the values of Wilson’s parameters were obtained in binary M-Al, M-Fe, and Al-Fe systems at 850 °C (Table 3).

**Table 2.** The calculation parameters of different alloying elements [31].

Element	$n_{ws}^{1/3}$ ((d.u.) <sup>1/3</sup> )	$\varphi$ (V)	$V^{2/3}$ (cm <sup>2</sup> )	$u$	$r/p$	$T_m$ (°C)
Al	1.39	4.20	4.64	0.07	1.9	660 [32]
Fe	1.77	4.93	3.69	0.04	1.0	1536 [33]
Cr	1.73	4.65	3.74	0.04	1.0	1875 [34]
Mn	1.61	4.45	3.78	0.04	1.0	1252 [35]
Co	1.75	5.10	3.50	0.04	1.0	1495 [34]
Ni	1.75	5.20	3.50	0.04	1.0	1455 [36]

**Table 3.** The calculated values of Wilson’s parameters in binary M-Al, M-Fe, and Al-Fe systems at 850 °C.

M (alloy)	$A_{M/Al}$	$A_{Al/M}$	$A_{M/Fe}$	$A_{Fe/M}$	$A_{Al/Fe}$	$A_{Fe/Al}$
Cr	−3.1812	−3.7626	−0.5424	−0.5546	−4.1184	−3.5930
Mn	−6.0446	−7.1179	0.0850	0.0840		
Co	−5.9119	−7.0274	−0.2059	−0.2147		
Ni	−7.0740	−8.3139	−0.5676	−0.5872		

The effect of M addition on the activity coefficient of Al and Fe atoms in the Al-2.47 at%Fe (Al-5wt%Fe) alloy at 850 °C, at the beginning stage of the chemical reaction in Equation (1), is shown in Figure 2. The results indicate that different alloying additions can result in different variations due to the distinct physical characteristics of M elements. With the M content increasing, the activity coefficient of Al decreases to different extents. On the contrary, the activity coefficient of Fe increase to different extents. In addition, Ni addition has a remarkable influence on the activity of Al and Fe, whereas Cr addition has little effect on the activity of Al and Fe. According to the values of activity coefficient, the activity of Al and Fe were obtained and are shown in Figure 3. The influence of M elements on the activity of Al and Fe is consistent with that of the activity coefficient of Al and Fe.

The nature of alloying elements significantly influenced the variation of Gibbs free energy, originating from the physical characteristics of the alloying elements (Figure 4). It can be seen that the Gibbs free energy of the chemical reaction decreases to different extents with different alloying additions. Moreover, with M element addition, the Gibbs free energy can be decreased and this is associated with the increased formation of Al<sub>13</sub>Fe<sub>4</sub>. The addition of Ni can significantly decrease the free energy and visibly promote the reaction. The Gibbs free energy of the reaction in Equation (1) provides a direct driving force for the formation of Al<sub>13</sub>Fe<sub>4</sub> phase which is the only product in the reaction. The results reveal that the incorporation of alloying elements reduced the Gibbs free energy and, in turn, increased the driving force for phase transition.

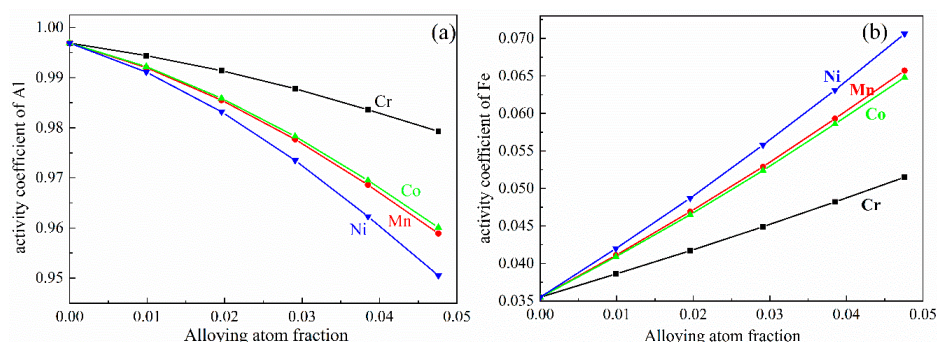


**Figure 2.** The activity coefficient of (a) Al and (b) Fe atoms in Al-2.47 at% Fe alloy melt at 850 °C.

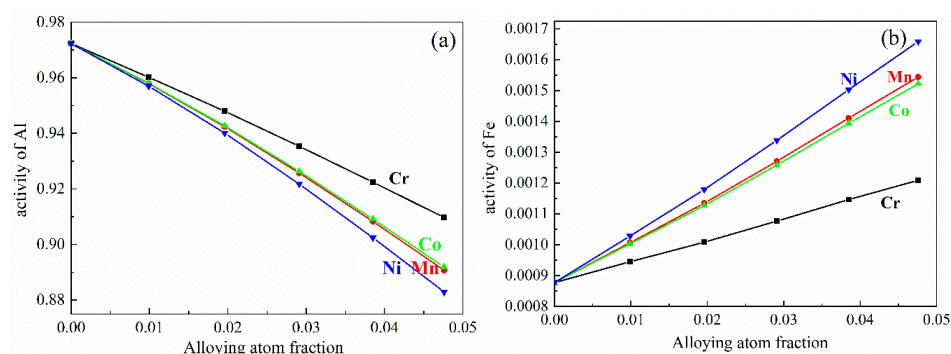


**Figure 3.** The activity of (a) Al and (b) Fe atoms in Al-2.47 at% Fe alloy melt at 850 °C.

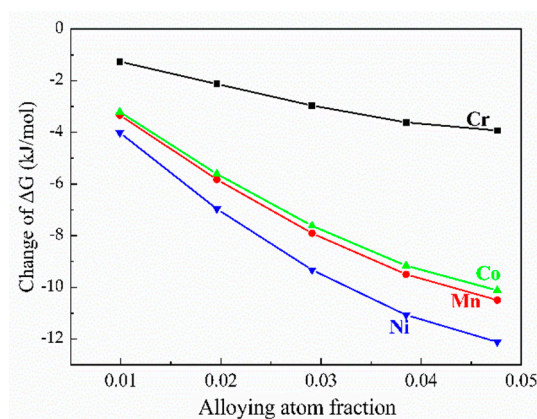


**Figure 4.** Influence of M content on the change in Gibbs free energy of  $Al_{13}Fe_4$  phase.

It is worth noting, that the precipitation of the  $Al_{13}Fe_4$  phase from the supersaturated solution of Al-2.47at% Fe melt represents a transition from the metastable phase to a stable phase, which is realized by the difference in Gibbs free energy. This difference in Gibbs free energy determines the speed of nucleation and growth. So, the change in Gibbs free energy influences the nucleation and growth of the  $Al_{13}Fe_4$  phase. On the one hand, according to the chemical reaction kinetics, the primary homogeneous nucleation rate can be expressed as [37]:

$$I = 10^2 \cdot \frac{nk_B T}{h} \cdot \exp(-\Delta G_c/k_B T) = 10^2 \cdot \frac{nk_B T}{h} \cdot \exp\left(-\frac{16\pi\sigma^3 V^2}{3k_B T \Delta G^2}\right), \quad (12)$$

where  $n$  represents the number of atoms in a liquid mass,  $k_B$  refers to the Boltzmann constant,  $\sigma$  corresponds to the interfacial energy per square decimeter between liquid and solid crystals,  $V$  denotes the volume of crystals and  $\Delta G_c$  refers to the free energy for critical nucleus formation. It indicates that the nucleation rate is exponentially related to the Gibbs free energy. It has no effect on the volume ( $V$ ) and Gibbs free energy for critical nucleus formation ( $\Delta G_c$ ) when 3D transition atoms are not involved in crystallization. Under the same number of 3D transition atoms ( $n$ ) in the melt, the interfacial energy per square decimeter can be considered equal, due to slight differences. So, Equation (12) shows that the change in Gibbs free energy only determines the primary homogeneous nucleation rate.

In the case of Al-2.47at%Fe melt, due to the low solubility of Fe in aluminum [38], the generalized equation for the growth of the crystal nucleus, according to the linear growth rate, can be given as:

$$v = A \cdot \Delta G \cdot \exp(b/T), \quad (13)$$

where  $A$  and  $b$  are system constants [38]. Overall, the nucleation rate is more sensitive to Gibbs free energy than the growth rate. The increase in the absolute value of Gibbs free energy ( $\Delta G < 0$ ) is conducive to grain refinement. On the other hand, it exhibits

a relationship of  $\Delta G = \Delta H_m - T_m \Delta S$  under solid–liquid equilibrium conditions. The phase transition begins at below the equilibrium temperature, exhibiting the following relationship [38]:

$$\Delta G = \Delta H - (T_m - \Delta T) \Delta S \approx \Delta H_m - T_m \Delta S + \Delta T \Delta S \approx \Delta T \Delta S, \quad (14)$$

where  $\Delta H_m$  and  $T_m$  represent the latent heat of phase change and crystallization temperature, respectively, and  $\Delta T$  refers to the subcooled degree. Under these conditions, the change in entropy ( $\Delta S$ ) can be regarded as a constant. Equation (14) indicates that the Gibbs free energy is proportional to the subcooled degree and the increase in the absolute value of the Gibbs free energy is conducive to an increase in the subcooled degree, which can promote the refinement of the  $\text{Al}_{13}\text{Fe}_4$  phase. Hence, it can be predicted that the incorporation of the M element is beneficial for promoting nucleation and refinement of the  $\text{Al}_{13}\text{Fe}_4$  phase, where Ni renders the most prominent influence, followed by Mn, Co and Cr.

### 3.2. Formation Enthalpy of $\text{Al}_{13}\text{Fe}_4$ Phase

In addition to the Gibbs free energy of the  $\text{Al}_{13}\text{Fe}_4$  phase, the incorporation of transition metal elements affected the formation enthalpy of the  $\text{Al}_{13}\text{Fe}_4$  phase by forming substitutional solid-solutions. The effect of M addition on the formation enthalpy of the  $\text{Al}_{13}\text{Fe}_4$  phase was assessed using the first-principle calculations. First, the  $\text{Al}_{13}\text{Fe}_4$  crystal was optimized to ensure the reliability of the calculations. The optimized lattice constants of the  $\text{Al}_{13}\text{Fe}_4$  crystal were  $a = 15.366 \text{ \AA}$ ,  $b = 8.012 \text{ \AA}$ ,  $c = 12.393 \text{ \AA}$  and  $\beta = 107.67^\circ$ , which are close to the previously reported values ( $a = 15.487 \text{ \AA}$ ,  $b = 8.0831 \text{ \AA}$ ,  $c = 12.476 \text{ \AA}$  and  $\beta = 107.72^\circ$ ) which was obtained from powder XRD [22].

To investigate the occupying tendency of the M element in the  $\text{Al}_{13}\text{Fe}_4$  phase, the formation enthalpy of  $\text{Al}_{78}(\text{Fe}_{23}\text{M})$  ( $M = \text{Cr, Mn, Co and Ni}$ ) was calculated and is shown in Figure 5. As Cr, Mn, Co, and Ni belong to the same row of the periodic table and lie next to each other, these elements exhibit a small difference in atomic radii. Hence, M elements easily substituted Fe-sites in the  $\text{Al}_{13}\text{Fe}_4$  phase. It has been reported that these four elements are more likely to occupy the Fe sites [39–42]. If M substitutes one Fe atom in the  $\text{Al}_{13}\text{Fe}_4$  unit cell, no phase transition occurs and the proportion of substituted atoms remains at ~0.98 at%. The lower value of formation enthalpy corresponds to the more stable crystal structure [43]. The negative values of formation enthalpy of  $\text{Al}_{78}(\text{Fe}_{23}\text{M})$  ( $M = \text{Cr, Mn, Co and Ni}$ ) indicate that the substituted compounds are thermodynamically stable. The formation enthalpy decreased in the given order:  $\text{Al}_{78}(\text{Fe}_{23}\text{Cr}) > \text{Al}_{78}(\text{Fe}_{23}\text{Mn}) > \text{Al}_{13}\text{Fe}_4 > \text{Al}_{78}(\text{Fe}_{23}\text{Ni}) > \text{Al}_{78}(\text{Fe}_{23}\text{Co})$ , where the formation enthalpy of  $\text{Al}_{78}(\text{Fe}_{23}\text{Ni})$  is comparable to the  $\text{Al}_{78}(\text{Fe}_{23}\text{Co})$  phase.

Additionally, the Cr and Mn preferred to occupy the Fe-5 site, whereas Co and Ni preferred the Fe-1 sites. Compared with Fe, the 3D orbitals of Co and Ni contain fewer electrons, which favors the occupation of Fe-1 site with a large coordination number, whereas the Cr and Mn occupy the Fe-5 position with a smaller coordination number. It can be inferred that the number of electrons in the 3D orbitals of transition metals critically influences the substitution position. It has been reported that the contribution of Fe in different positions at the Fermi level is different, which is related to the difference in the coordination number [44–46]. The inter-atomic bonding process is exothermic [47]. Therefore, the larger coordination number corresponds to the higher bonding degree and better stability. The addition of Co and Ni decreased the formation enthalpy by occupying the Fe-1 position with a large coordination number. Additionally, the formation of several bonds is more conducive to increasing compound stability.

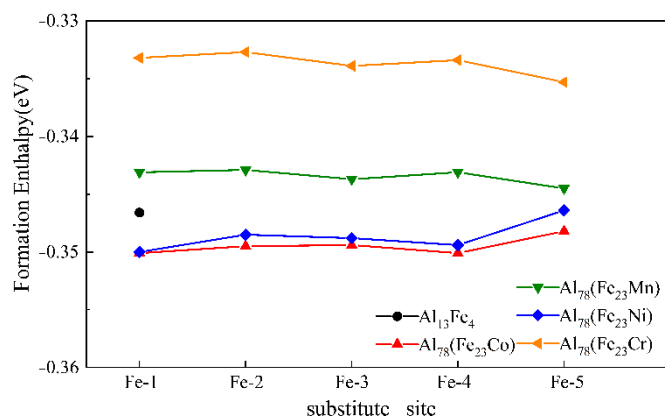


**Figure 5.** The formation enthalpy of  $\text{Al}_{13}\text{Fe}_4$  and  $\text{Al}_{78}(\text{Fe}_{23}\text{M})$  phases, where  $\text{M} = \text{Cr}, \text{Mn}, \text{Co}$  and  $\text{Ni}$ .

On the other hand, the addition of Cr and Mn increased the formation enthalpy of the compound and decreased its stability. The replacement of Fe-5 positions with a smaller coordination number and fewer bonds is more conducive to slowing down the increase in formation enthalpy. Based on the formation enthalpy results, the interatomic forces of the compounds, which are formed after the substitution of Cr and Mn, are reduced, where the bond length of Al-M is found to be higher than that of Al-Fe. Additionally, the stability of  $\text{Al}_{78}(\text{Fe}_{23}\text{Cr})$  and  $\text{Al}_{78}(\text{Fe}_{23}\text{Mn})$  compounds is compromised, and both Cr and Mn are more likely to occupy the Fe-5 position. On the other hand, the interatomic forces of  $\text{Al}_{78}(\text{Fe}_{23}\text{Ni})$  and  $\text{Al}_{78}(\text{Fe}_{23}\text{Co})$  compounds, which are formed after Ni and Co substitution, are enhanced and the Al-M bond length became shorter than the Al-Fe. Moreover, the thermal stability of  $\text{Al}_{78}(\text{Fe}_{23}\text{Ni})$  and  $\text{Al}_{78}(\text{Fe}_{23}\text{Co})$  compounds is increased, and both Ni and Co preferred to occupy the Fe-I position with a large influence on the overall energy.

The lattice constants of the  $\text{Al}_{13}\text{Fe}_4$  and  $\text{Al}_{78}(\text{Fe}_{23}\text{M})$  phases, with  $\text{M} = \text{Cr}, \text{Mn}, \text{Co}$  and  $\text{Ni}$ , which possesses the highest negative value of formation enthalpy, are shown in Table 4. It can be readily observed that the introduction of M elements induced lattice distortions and increased the unit cell volume. The increase in unit cell volume remained consistent with the atomic radii of M elements. It is worth noting that, in addition to the  $\text{Al}_{78}(\text{Fe}_{23}\text{Co})$  phase, the formation enthalpy and volume change trends of  $\text{Al}_{78}(\text{Fe}_{23}\text{M})$  phases ( $\text{M} = \text{Cr}, \text{Mn}, \text{Ni}$ ) are consistent with the change in atomic radii of M elements. If only the effect of atomic radius on volume is considered, the volume of  $\text{Al}_{78}(\text{Fe}_{23}\text{Co})$  should be larger than the  $\text{Al}_{78}(\text{Fe}_{23}\text{Ni})$  phase, which is contrary to our current results. Hence, compared with the atomic radii, the formation enthalpy plays a more prominent role in defining the volume of a unit cell. It has been reported that the monoclinic phases of  $\text{Al}_{13}\text{Co}_4$  and  $\text{Al}_{13}\text{Fe}_4$  possess similar crystallographic structures and may form a continuous solid-solution of  $\text{Al}_{13}(\text{Fe},\text{Co})_4$  [28,48], which is not observed in the case of other transition metals. The experimental and theoretical studies revealed that the formation enthalpy of  $\text{Al}_{13}\text{Co}_4$  is more negative than the  $\text{Al}_{13}\text{Fe}_4$  phase [49]. This can be the reason for the lower formation enthalpy and a smaller volume of  $\text{Al}_{78}(\text{Fe}_{23}\text{Co})$  phase than the  $\text{Al}_{78}(\text{Fe}_{23}\text{M})$  phase ( $\text{M} = \text{Cr}, \text{Mn}$  and  $\text{Ni}$ ). Hence, the incorporation of 3D transition elements changed the lattice constants of the  $\text{Al}_{13}\text{Fe}_4$  phase in different degrees, but this change is small enough to cause a change in the symmetry of lattice structure.

**Table 4.** The lattice constants of  $\text{Al}_{13}\text{Fe}_4$  and  $\text{Al}_{78}(\text{Fe}_{23}\text{M})$  phases, where  $\text{M} = \text{Cr}, \text{Mn}, \text{Co}$ , and  $\text{Ni}$ .

Compound	$a$ (Å)	$b$ (Å)	$c$ (Å)	$V_{cell}$ (Å <sup>3</sup> )
$\text{Al}_{13}\text{Fe}_4$	15.366	8.012	12.393	1453.9
$\text{Al}_{78}(\text{Fe}_{23}\text{Ni})$	15.367	8.027	12.385	1455.3
$\text{Al}_{78}(\text{Fe}_{23}\text{Co})$	15.355	8.020	12.392	1454.1
$\text{Al}_{78}(\text{Fe}_{23}\text{Mn})$	15.393	8.005	12.396	1455.5
$\text{Al}_{78}(\text{Fe}_{23}\text{Cr})$	15.383	8.023	12.413	1459.5

According to the thermodynamic driving force for phase transitions, the Gibbs free energy under isobaric conditions can be expressed as:

$$G(t) = H(T) - TS(T), \quad (15)$$

Herein, solidification precipitation of the  $\text{Al}_{13}\text{Fe}_4$  phase from the Al-Fe alloy liquid phase requires a driving force of  $\Delta G < 0$  ( $\Delta G = \Delta H - T\Delta S$ ). When M replaces one Fe atom under the same temperature and concentration, the slight increase in  $\Delta S$  can be considered as a constant in the  $\text{Al}_{78}(\text{Fe}_{23}\text{M})$  phase. It can be predicted that the decrease in formation enthalpy increases the driving force for phase transition after forming  $\text{Al}_{78}(\text{Fe}_{23}\text{Ni})$  and  $\text{Al}_{78}(\text{Fe}_{23}\text{Co})$  phases, which is more conducive to promoting nucleation and refinement of the  $\text{Al}_{13}\text{Fe}_4$  phase. Additionally, the compromised stability promotes the formation of other metastable phases, such as  $\text{Al}_6\text{Fe}$ , in the Al-Fe alloy after the substitution of Cr and Mn. One should note that the formation of the metastable  $\text{Al}_x\text{Fe}$  phase in Al-Fe alloys due to the addition of Cr and Mn has been reported [13,41].

### 3.3. Influence of M Addition on Microstructural Evolution

Furthermore, we have selected Al-5wt%Fe-1wt%Cr and Al-5wt%Fe-1wt%Ni alloys, with the minimum and maximum change in Gibbs free energy of  $\text{Al}_{13}\text{Fe}_4$  phase, and studied the microstructural evolution due to the addition of M element (Figure 6). The length distribution chart of  $\text{Al}_{13}\text{Fe}_4$  is shown in Figure 7. The length of the primary  $\text{Al}_{13}\text{Fe}_4$  phase ranges from 10 to 200  $\mu\text{m}$ , which includes some very large coarse grains. The value of the average length is 43.10  $\mu\text{m}$ . The addition of Ni greatly refined the grains of primary  $\text{Al}_{13}\text{Fe}_4$  phase (Figure 6b), and the average length of primary  $\text{Al}_{13}\text{Fe}_4$  phase ranges from 5 to 70  $\mu\text{m}$ . The value of the average length is 27.75  $\mu\text{m}$ , whereas the addition of Cr only slightly refined the grains of primary  $\text{Al}_{13}\text{Fe}_4$  phase (Figure 6c). The value of the average length is 39.25  $\mu\text{m}$ . This is consistent with our previous analysis on the effect of alloying elements, showing that Ni renders the most prominent refinement effect. The mechanism of grain refinement from a thermodynamics viewpoint clearly revealed the experimental phenomena.

Figure 8 presents XRD patterns of the as-cast Ni- and Cr-added alloys. The Al-5wt%Fe-1wt%Ni alloy consisted of  $\alpha$ -Al,  $\text{Al}_{13}\text{Fe}_4$ ,  $\text{Al}_9\text{FeNi}$ , and  $\text{Al}_3\text{Ni}$  phases in the as-cast state (Figure 8a), whereas Al-5wt%Fe-1wt%Cr alloy consisted of  $\alpha$ -Al,  $\text{Al}_{13}\text{Fe}_4$ , and  $\text{Al}_{13}\text{Cr}_2$  phases in the as-cast state (Figure 8b). The added M element partially formed the secondary compound with Al and promoted heterogeneous nucleation of the  $\alpha$ -Al phase. The remaining amount of M element was dissolved in the  $\text{Al}_{13}\text{Fe}_4$  phase, which leads to grain refinement and microstructural changes. The EDS results confirm the presence of Fe, Cr and Ni atoms in  $\alpha$ -Al grains (Point-A and Point-D), as shown in Figures 9 and 10. One should note that the solid-solubility of M elements in  $\alpha$ -Al is extremely small, whereas the solid-solubility of Cr and Ni in the primary  $\text{Al}_{13}\text{Fe}_4$  phase is relatively large (Point-B and Point-E). As the amount of eutectic  $\text{Al}_{13}\text{Fe}_4$  phase is relatively small and the formation temperature is low, a small amount of Cr element was dissolved in the  $\text{Al}_{13}\text{Fe}_4$  phase (Point-C). Moreover, the  $\text{Al}_9\text{FeNi}$  phase was distributed at grain boundaries in the form of layers (Point-F), however, its influence on the  $\text{Al}_{13}\text{Fe}_4$  phase will be studied later.

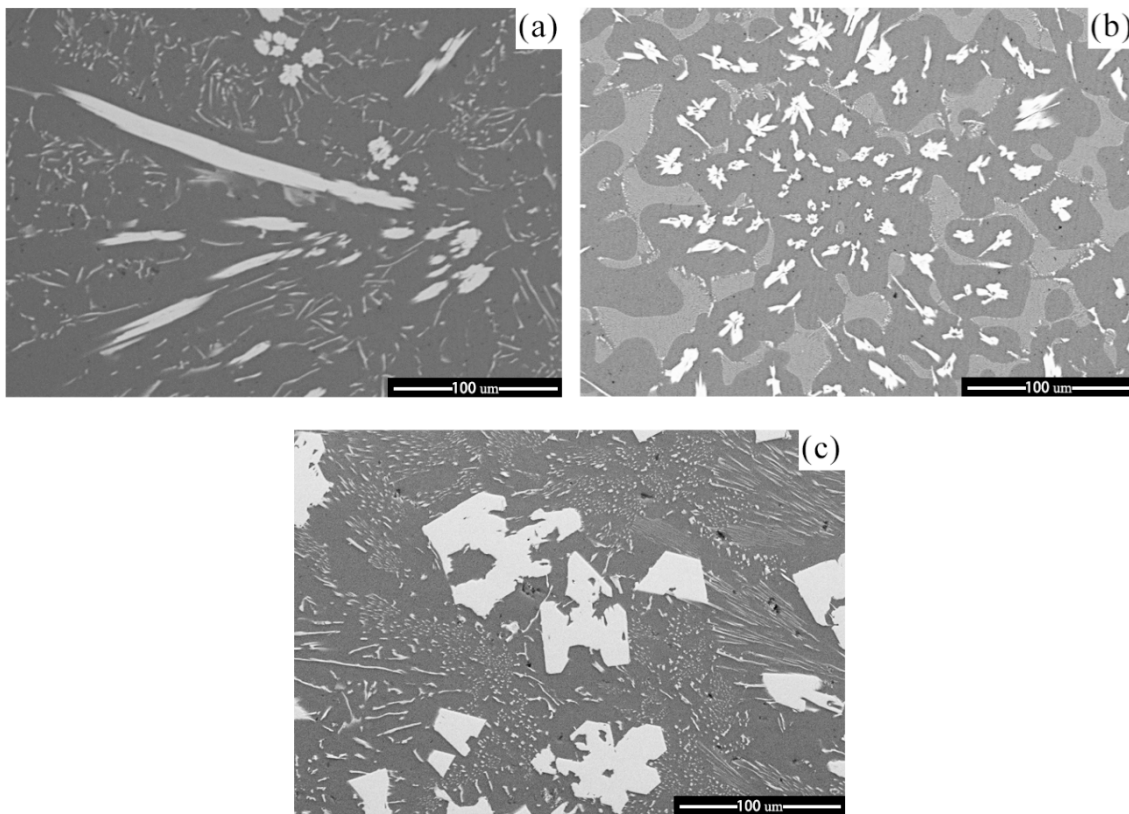


**Figure 6.** The as-cast microstructure of (a) Al-5wt%Fe, (b) Al-5wt%Fe-1wt%Ni and (c) Al-5wt%Fe-1wt%Cr.

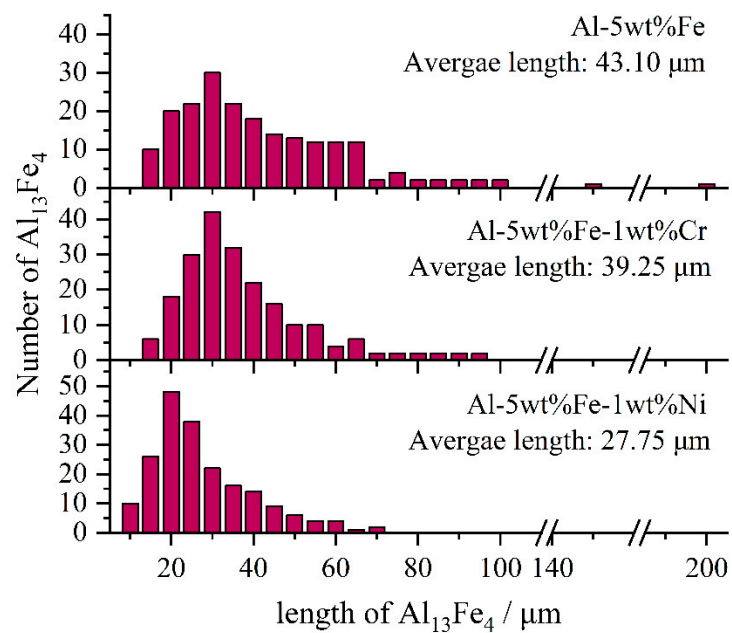


**Figure 7.** Lengths distribution of  $Al_{13}Fe_4$  in Al-5wt%Fe-M alloys.

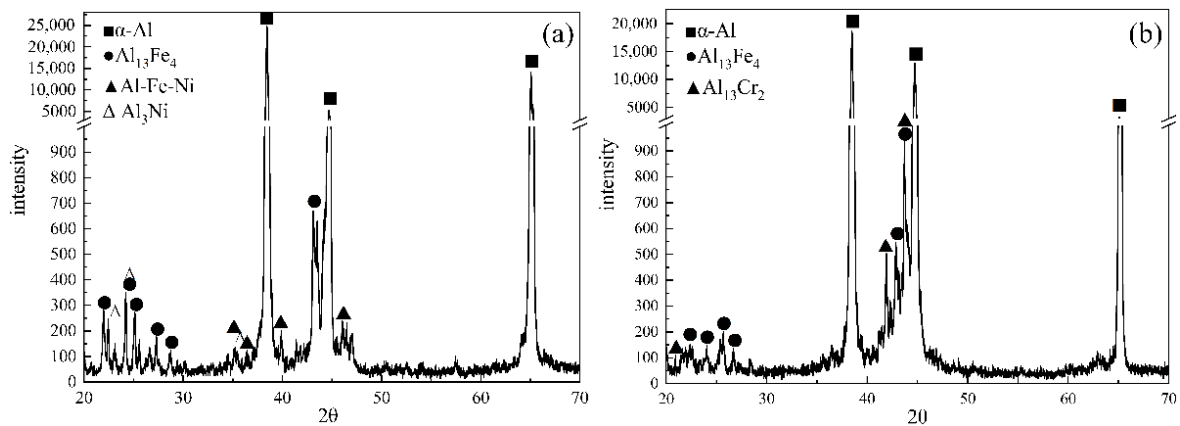


Figure 8. XRD patterns of as-cast alloys: (a) Al-5wt%Fe-1wt%Ni and (b) Al-5wt%Fe-1wt%Cr.

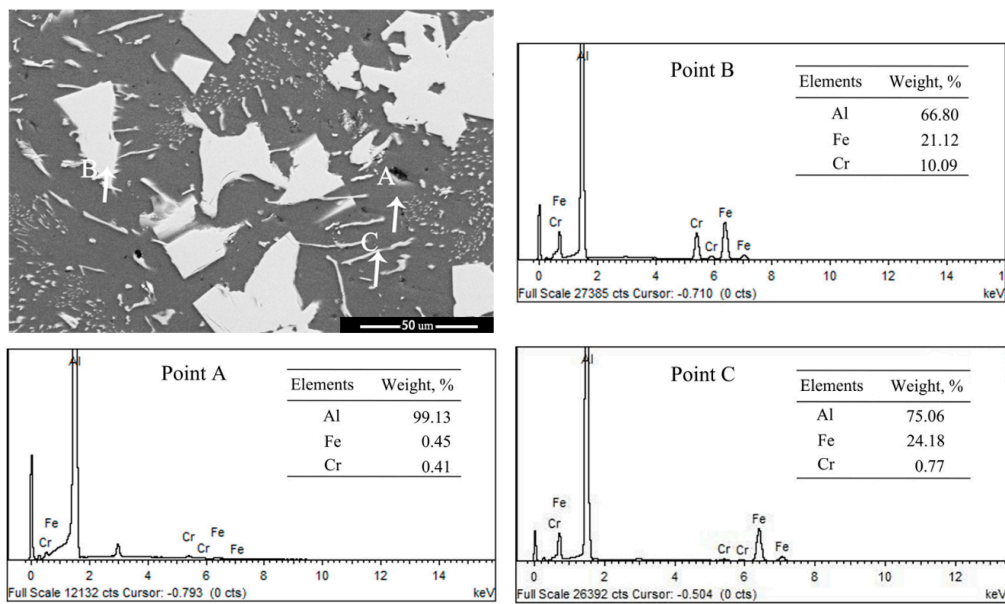


Figure 9. SEM image and corresponding EDS spectra of Point-A, -B and -C of Al-5wt%Fe-1wt%Cr alloy.

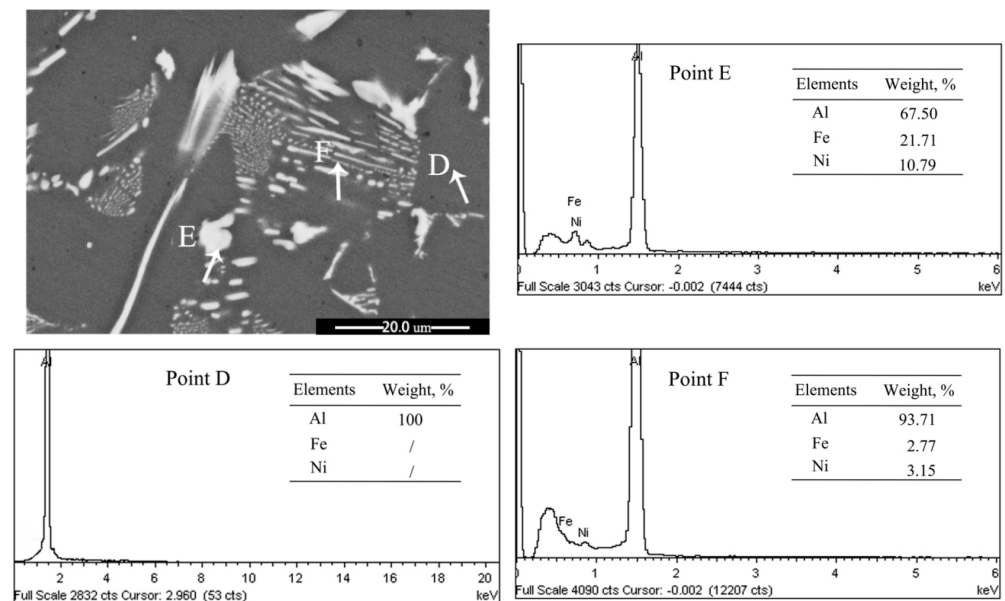


Figure 10. SEM image and corresponding EDS spectra of Point-D, -E and -F of Al-5wt%Fe-1wt%Ni alloy.

#### 4. Conclusions

In summary, the current study aimed to reveal the mechanism of grain refinement of an  $\text{Al}_{13}\text{Fe}_4$  phase due to the addition of 3D transition elements, from a thermodynamics viewpoint. The main conclusions of the current study can be summarized as:

(1) M addition increased the activity and effective concentration of Fe, whereas it reduced the activity of Al in Al-Fe alloy melt. Additionally, the incorporation of M elements reduced the Gibbs free energy and increased the driving force for phase transition, promoting the nucleation and refinement of the  $\text{Al}_{13}\text{Fe}_4$  phase. Moreover, Ni addition rendered the most prominent influence, followed by Mn, Co, and Cr.

(2) The formation enthalpy decreased in the following order:  $\text{Al}_{78}(\text{Fe}_{23}\text{Cr}) > \text{Al}_{78}(\text{Fe}_{23}\text{Mn}) > \text{Al}_{13}\text{Fe}_4 > \text{Al}_{78}(\text{Fe}_{23}\text{Ni}) > \text{Al}_{78}(\text{Fe}_{23}\text{Co})$ , where the formation enthalpy of  $\text{Al}_{78}(\text{Fe}_{23}\text{Ni})$  was comparable to the  $\text{Al}_{78}(\text{Fe}_{23}\text{Co})$ . Additionally, Cr and Mn preferred to occupy the Fe-5 sites, whereas Co and Ni preferred to occupy the Fe-1 sites. Overall, the decrease in formation enthalpy increased the driving force of the phase transition after forming  $\text{Al}_{78}(\text{Fe}_{23}\text{Ni})$  and  $\text{Al}_{78}(\text{Fe}_{23}\text{Co})$  phases, which was more conducive to promoting the nucleation and refinement of the  $\text{Al}_{13}\text{Fe}_4$  phase. Moreover, the compromised stability of  $\text{Al}_{78}(\text{Fe}_{23}\text{Cr})$  and  $\text{Al}_{78}(\text{Fe}_{23}\text{Mn})$  phases promoted the formation of other metastable phases, e.g.,  $\text{Al}_6\text{Fe}$ , in the Al-Fe alloy after the substitution of Cr and Mn.

(3) The comparison of Al-5wt%Fe-1wt%Cr and Al-5wt%Fe-1wt%Ni alloys revealed that the addition of Ni significantly refined the  $\text{Al}_{13}\text{Fe}_4$  phase, whereas Cr mainly improved the morphology of the  $\text{Al}_{13}\text{Fe}_4$  phase without refining the grains of the  $\text{Al}_{13}\text{Fe}_4$  phase.

These preliminary results demonstrate that the selection of an optimal alloying element to promote nucleation and refinement, is of great significance to further understand the grain refinement mechanism and provide theoretical bases for the application of M-doped Al-Fe alloys.

**Author Contributions:** Conceptualization, N.P. and Z.S.; methodology, C.W. and N.P.; validation, Z.S.; formal analysis, N.P.; investigation, Y.L. and N.L.; resources, Z.S.; data curation, C.W.; writing—original draft preparation, N.P.; writing—review and editing, N.P.; supervision, Z.S. All authors have read and agreed to the published version of the manuscript.

**Funding:** This research was funded by the Inner Mongolia Science and Technology Plan, China, grant number 2018-01-068 and the Key Discipline Team Project of Materials Science, Inner Mongolia University of Technology, grant number ZD202012.

**Data Availability Statement:** Data is contained within the article.

**Acknowledgments:** The authors thank Er-jun Zhao for providing computing resources and valuable discussion.

**Conflicts of Interest:** The authors declare no conflict of interest.

#### References

1. Goulart, P.R.; Cruz, K.S.; Spinelli, J.E.; Ferreira, I.L.; Cheung, N.; Garcia, A. Cellular growth during transient directional solidification of hypoeutectic Al-Fe alloys. *J. Alloys Compd.* **2009**, *470*, 589–599. [[CrossRef](#)]
2. Wang, J.; Zhou, Y.L.; He, M.Y.; Xu, L.; Wangyang, P.H. Thermal plasma jet approach towards the controllable preparation of Al-Fe alloys with high Fe content and spherical second phase. *J. Alloys Compd.* **2018**, *737*, 14–20. [[CrossRef](#)]
3. Liang, D.; Korgui, P.; Jones, H. Composition and solidification microstructure selection in the interdendritic matrix between primary  $\text{Al}_3\text{Fe}$  dendrites in hypereutectic Al-Fe Alloy. *Acta Mater.* **1996**, *44*, 2999–3004. [[CrossRef](#)]
4. Chen, J.; Lengsdorf, R.; Henein, H.; Herlach, D.M.; Dahlborg, U.; Calvo-Dahlborg, M. Microstructure evolution in undercooled Al-8wt%Fe melts: Comparison between terrestrial and parabolic flight conditions. *J. Alloys Compd.* **2013**, *556*, 243–251. [[CrossRef](#)]
5. Goulart, P.R.; Spinelli, J.E.; Cheung, N.; Garcia, A. The effects of cell spacing and distribution of intermetallic fibers on the mechanical properties of hypoeutectic Al-Fe alloys. *Mater. Chem. Phys.* **2010**, *119*, 272–278. [[CrossRef](#)]
6. Premkumar, M.K.; Lawley, A.; Koczak, M.J. Processing and microstructure of powder metallurgy Al-Fe-Ni alloys. *Metall. Trans. A* **1992**, *23*, 3219–3230. [[CrossRef](#)]
7. Hatayama, H.; Daigo, I.; Matsuno, Y.; Adachi, Y. Assessment of the recycling potential of Aluminum in Japan, the United States, Europe and China. *Mater. Trans.* **2009**, *50*, 450–456. [[CrossRef](#)]

8. Voděrová, M.; Novák, P.; Marek, I.; Vojtěch, D. Microstructure and mechanical properties of rapidly solidified Al-Fe-X alloys. *Key Eng. Mater.* **2013**, *592–593*, 639–642. [[CrossRef](#)]
9. Voděrová, M.; Novák, P.; Marek, I.; Vojtěch, D. Microstructure of rapidly solidified and hot-pressed Al-Fe-X Alloys. *Mater. Technol.* **2014**, *48*, 349–353.
10. Manuel, V.C.; Crystopher, B.; Spinelli, J.E.; Garcia, A. Interrelation of cell spacing, intermetallic compounds and hardness on a directionally solidified Al–1.0Fe–1.0Ni alloy. *Mater. Des.* **2013**, *51*, 342–346.
11. Průša, F.; Vojtěch, D.; Michalcová, A.; Marek, I. Mechanical properties and thermal stability of Al–Fe–Ni alloys prepared by centrifugal atomization and hot extrusion. *Mater. Sci. Eng. A* **2014**, *603*, 141–149. [[CrossRef](#)]
12. Soustani, M.F.; Taghiabadi, R.; Jafarzadegan, M.; Farahan, M.V. Effect of multi-pass friction stir processing on microstructure and mechanical properties of cast Al-7Fe-5Ni alloy. *Mater. Res. Express* **2019**, *10*, 1–14. [[CrossRef](#)]
13. Liu, B.; Yuan, X.G.; Huang, H.J.; Guo, Z.Q. The effect of alloying elements on the microstructure of Al-5Fe Alloys. *JOM-J. Miner. Met. Mater. Soc.* **2012**, *64*, 316–322. [[CrossRef](#)]
14. Yan, F.; Kumar, S.; McKay, B.J.; O'Reilly, K.A.Q. Effect of Mn on Fe containing phase formation in high purity aluminum. *Int. J. Cast. Met. Res.* **2014**, *27*, 202–206. [[CrossRef](#)]
15. Zhou, Z.P.; Li, R.D.; Ma, J.C.; Yu, H.S. Effect of Co on As-cast Microstructure of Al-5%Fe Alloy. *J. Mater. Eng.* **2005**, *2*, 54–58.
16. Fan, T.X.; Yang, G.; Zhang, D. Prediction of chemical stability in SiCp/Al composites with alloying element addition using Wilson equation and an extended Miedema model. *Mat. Sci. Eng. A* **2005**, *394*, 327–338. [[CrossRef](#)]
17. Fan, T.X.; Yang, G.; Zhang, D. Thermodynamic effect of alloying addition on in-situ reinforced TiB<sub>2</sub>/Al composites. *Metall. Mater. Trans. A* **2005**, *36*, 225–234. [[CrossRef](#)]
18. Zhang, C.F.; Fan, T.X.; Cao, W.; Zhang, D. A model for work of solid-liquid adhesion in multicomponent melts. *Acta Mater.* **2009**, *57*, 3623–3632. [[CrossRef](#)]
19. Wilson, G.M. Vapor-Liquid equilibrium XI. A new expression for the excess free energy of mixing. *J. Am. Chem. Soc.* **1964**, *86*, 127–130. [[CrossRef](#)]
20. Miedema, A.R.; de Chatel, P.F.; de Boer, F.R. Cohesion in alloys—Fundamental of a semi-empirical model. *Phys. B* **1980**, *100*, 1–28. [[CrossRef](#)]
21. Zhang, C.F.; Fan, T.X.; Cao, W.; Ding, J.; Zhang, D. Size control of in situ formed reinforcement in metal melts—theoretical treatment and application to in situ (AlN+Mg<sub>2</sub>Si)/Mg composites. *Compos. Sci. Technol.* **2009**, *69*, 2688–2694. [[CrossRef](#)]
22. Black, P.J. The structure of FeAl<sub>3</sub>.I. *Acta Cryst.* **1995**, *8*, 43–48. [[CrossRef](#)]
23. Black, P.J. The structure of FeAl<sub>3</sub>.II. *Acta Cryst.* **1995**, *8*, 175–182. [[CrossRef](#)]
24. Grin, J.; Burkhardt, U.; Ellner, M.; Peters, K. Refinement of the Fe<sub>4</sub>Al<sub>13</sub> structure and its relationship to the quasihomological homeotypical structures. *Z. Kristallogr.* **1994**, *209*, 479–487. [[CrossRef](#)]
25. Segall, M.D.; Lindan, P.J.; Probert, M.J.; Pickard, C.J.; Hasnip, P.J.; Clark, S.J.; Payne, M.C. First-principles simulation: Ideas, illustration and the CASTEP code. *J. Phys. Condens. Matter.* **2002**, *14*, 2717–2744. [[CrossRef](#)]
26. Perdew, J.P.; Burke, K.; Ernzerhof, M. Generalized Gradient Approximation Made Simple. *Phys. Rev. Lett.* **1996**, *77*, 3865–3868. [[CrossRef](#)]
27. Vanderbilt, D. Soft self-consistent pseudopotentials in a generalized eigenvalue formalism. *Phys. Rev. B* **1990**, *41*, 7892–7895. [[CrossRef](#)]
28. Monkhorst, H.J.; Pack, J.D. Special points for Brillouin-zone integrations. *Phys. Rev. B* **1976**, *16*, 1748–1749. [[CrossRef](#)]
29. Owen, E.A.; Preston, G.D. The atomic structure of two intermetallic compounds. *Proc. Phys. Soc.* **1924**, *36*, 341–348. [[CrossRef](#)]
30. Piccolo, L.; Chatelier, C.; Weed, M.; Morfin, F.; Ledieu, J.; Fournée, V.; Gille, P.; Gaudry, E. Catalytic properties of Al<sub>13</sub>TM<sub>4</sub> complex intermetallics: Influence of the transition metal and the surface orientation on butadiene hydrogenation. *Sci. Technol. Adv. Mater.* **2019**, *20*, 557–567. [[CrossRef](#)]
31. Miedema, A.R.; de Boer, F.R.; Boom, R. Model predictions for the enthalpy of formation of transition metal alloys. *Calphad* **1983**, *7*, 51–70. [[CrossRef](#)]
32. Boehler, R.; Ross, M. Melting curve of aluminum in a diamond cell to 0.8 Mbar: Implications for iron. *Earth and Planet. Sci. Lett.* **1997**, *153*, 223–227.
33. Boehler, R.; Santamaria Pérez, D.; Errandonea, D.; Mezouar, M. Melting, density, and anisotropy of iron at core conditions: New x-ray measurements to 150 GPa. *J. Phys. Conf. Ser.* **2008**, *121*, 022018. [[CrossRef](#)]
34. Errandonea, D.; Schwager, B.; Ditz, R.; Gessmann, C.; Boehler, R.; Ross, M. Systematics of transition-metal melting. *Phys. Rev. B* **2001**, *63*, 849–853. [[CrossRef](#)]
35. Errandonea, D. The melting curve of ten metals up to 12 GPa and 1600 K. *J. Appl. Phys.* **2010**, *108*, 033517. [[CrossRef](#)]
36. Errandonea, D. High-pressure melting curves of the transition metals Cu, Ni, Pd, and Pt. *Phys. Rev. B* **2013**, *87*, 054108. [[CrossRef](#)]
37. Turnbull, D. Formation of crystal nuclei in liquid metals. *J. Appl. Phys.* **1950**, *21*, 1022–1028. [[CrossRef](#)]
38. Zhang, K.C.; Zhang, L.H. The thermodynamic basis and nucleation theory of crystal growth. In *Crystal Growth*, 1st ed.; Science Press: Beijing, China, 1981; pp. 51–68. (In Chinese)
39. Popčević, P.; Smontara, A.; Ivkov, J.; Wencka, M.; Komelj, M.; Jeglič, P.; Vrtnik, S.; Bobnar, M.; Jagličić, Z.; Bauer, B.; et al. Anisotropic physical properties of the Al<sub>13</sub>Fe<sub>4</sub> complex intermetallic and its ternary derivative Al<sub>13</sub>(Fe, Ni)<sub>4</sub>. *Phys. Rev. B* **2010**, *81*, 1–12. [[CrossRef](#)]

40. Marlena, O.; Cacciamani, G. Critical evaluation and thermodynamic modeling of the Al-Co-Fe system. *J. Alloys Compd.* **2019**, *794*, 553–568.
41. Bauer, B.; Gille, P. Crystal Growth of Al-Rich Complex Metallic Phases in the System Al-Cr-Fe Using the Czochralski Method. *Z. Anorg. Allg. Chem.* **2011**, *637*, 2052–2058. [[CrossRef](#)]
42. Zheng, W.S.; Mao, H.H.; Lu, X.G.; He, Y.L.; Li, L.; Selleby, M.L.; Ågren, J. Thermodynamic investigation of the Al-Fe-Mn system over the whole composition and wide temperature ranges. *J. Alloys Compd.* **2018**, *742*, 1046–1057. [[CrossRef](#)]
43. Zoroddu, A.; Bernardini, F.; Ruggerone, P.; Fiorentini, V. First-principles prediction of structure, energetics, formation enthalpy, elastic constants, polarization, and piezoelectric constants of AlN, GaN, and InN: Comparison of local and gradient-corrected density-functional theory. *Phys. Rev. B* **2000**, *64*, 314–319. [[CrossRef](#)]
44. Yamada, T.; Kojima, T.; Kameoka, S.; Murakami, Y.; Gille, P.; Tsai, A.P. Probing Single Pt Atoms in Complex Intermetallic Al<sub>13</sub>Fe<sub>4</sub>. *J. Am. Chem. Soc.* **2018**, *140*, 3838–3841. [[CrossRef](#)] [[PubMed](#)]
45. Ullah, I.; Mehmood, S.; Ali, Z.; Rehman, G.; Khan, I.; Ahmad, I. Theoretical studies of the electronic structure and magnetic properties of aluminum-rich intermetallic alloy Al<sub>13</sub>Fe<sub>4</sub>. *Int. J. Mod. Phys. B* **2018**, *32*, 1850201. [[CrossRef](#)]
46. Albedah, M.A.; Nejadstari, F.; Stadnik, Z.M.; Przewoznik, J. Fe-57 Mossbauer spectroscopy and magnetic study of Al<sub>13</sub>Fe<sub>4</sub>. *J. Alloys Compd.* **2015**, *619*, 839–845. [[CrossRef](#)]
47. Huang, L.F.; Grabowski, B.; McEniry, E.; Trinkle, D.R.; Neugebauer, J. Importance of coordination number and bond length in titanium revealed by electronic structure investigations. *Phys. Status Solidi B* **2015**, *252*, 1907–1924. [[CrossRef](#)]
48. Zhu, L.L.; Soto-Medina, S.; Hennig, R.G.; Manuel, M.V. Experimental investigation of the Al-Co-Fe phase diagram over the whole composition range. *J. Alloys Compd.* **2020**, *815*, 152110. [[CrossRef](#)]
49. Gaudry, É.; Chatelier, C.; Loffreda, D.; Kandaskalov, D.; Coatib, A.; Piccolo, L. Catalytic activation of a non-noble intermetallic surface through nanostructuring under hydrogenation conditions revealed by atomistic thermodynamics. *J. Mater. Chem. A* **2020**, *8*, 7422–7431. [[CrossRef](#)]